Open access • Journal Article • DOI:10.1007/S00604-018-3104-Z

# Orthogonal gas sensor arrays by chemoresistive material design. — Source link

Nicolay J. Pineau, Julia F Kompalla, Andreas T. Güntner, Sotiris E. Pratsinis

**Institutions:** ETH Zurich

**Published on:** 28 Nov 2018 - Mikrochimica Acta (Springer Vienna)

# Orthogonal gas sensor arrays by chemoresistive material design

# Orthogonal gas sensor arrays by chemoresistive material design

Nicolay J. Pineau, Julia F. Kompalla, Andreas T. Güntner* and Sotiris E. Pratsinis

Particle Technology Laboratory, Department of Mechanical and Process Engineering, ETH Zurich, CH-8092 Zurich, Switzerland

*Microchimica Acta*

*submitted in Sept. 2018*

*and in revised form in Nov. 2018*

*corresponding author: andreas.guentner@ptl.mavt.ethz.ch

# Abstract

Gas sensor arrays often lack discrimination power to different analytes and robustness to interferants, limiting their success outside of research laboratories. This is primarily due to the widely sensitive (thus weakly-selective) nature of the constituent sensors. Here, the effect of *orthogonality* on array accuracy and precision by *selective sensor design* is investigated. Therefore, arrays of (2 – 5) *selective* and *non-selective* sensors are formed by systematically altering array size and composition. Their performance is evaluated with 60 random combinations of ammonia, acetone and ethanol at ppb to low ppm concentrations. Best analyte predictions with high coefficients of determination ($R^2$) of 0.96 for ammonia, 0.99 for acetone and 0.88 for ethanol are obtained with an array featuring high degree of orthogonality. This is achieved by using distinctly selective sensors (Si:$MoO_3$ for ammonia and Si:$WO_3$ for acetone together with Si:$SnO_2$) that improve discrimination power and stability of the regression coefficients. On the other hand, arrays with collinear sensors (Pd:$SnO_2$, Pt:$SnO_2$ and Si:$SnO_2$) hardly improve gas predictions having $R^2$ of 0.01, 0.86 and 0.28 for ammonia, acetone and ethanol, respectively. Sometimes they even exhibited lower coefficient of determination than single sensors as a Si:$MoO_3$ sensor alone predicts ammonia better with a $R^2$ of 0.68.



# Keywords

Gas sensor, ethanol, acetone, ammonia, $SnO_2$, $MoO_3$, $WO_3$, flame spray pyrolysis, electronic nose

# 1. Introduction

Since the introduction of gas sensor arrays in 1982 [1], they have been tested in numerous fields but still suffer from weak sensitivity and selectivity in gas mixtures [2]. As a result, the often applied "black box" approach correlating sensor signals with chemical perception (e.g., woody taste of wine) holds high risk of bogus correlations as the relevant analyte, responsible for the actual odor, aroma or disease, might not be generating the sensor outputs [2]. For instance when distinguishing alcoholic beverages, the sensor responses may primarily reflect variations in ethanol concentrations instead of wine aromas [3]. Similarly in breath analysis, the residues of tobacco smoke might be responsible for the diagnosis of lung cancer rather than actual markers [4]. This is important as lung cancer patients are most likely active or ex-smokers. As a consequence, it is essential to *quantify* the relevant analytes in the gas mixture. For example in breath analysis, this means a targeted analysis of markers with *proven biochemical relation* to the disease [5].

To address this, a sensor array consisting of four flame-made and differently doped (Pd, Pt, Ti and Si) $SnO_2$ sensors has been successfully applied to *quantify* formaldehyde in 4-analyte mixtures of main constituents of human breath at random concentrations [6]. The array quantified formaldehyde concentrations with an average estimation error of 9 ppb in the relevant range (30-180 ppb) despite much higher interferant levels (up to 2000 ppb ammonia, 1800 ppb acetone and 600 ppb ethanol). The interferants, however, were estimated with higher errors, for instance ammonia with 235 ppb [6]. Apparently, the widely sensitive (thus weakly selective) character of the applied $SnO_2$-based [6] sensors exhibited too small discrimination power to accurately resolve all compounds in the mixtures. This is problematic especially at relevant sub-ppm concentrations, where $SnO_2$-based arrays are rarely tested [7].

To increase the discrimination power and reduce cross-sensitivity to interferants, sensors with distinct selectivities are required [8]. Ideally, they combine to an array with *orthogonal*

characteristics enhancing discrimination power and estimation stability. This would improve precision and accuracy allowing for simultaneous quantification of multiple analytes as had been shown theoretically [9]. Distinct selectivity can be achieved by tailoring specific materials at the nanoscale (e.g. particle size, shape and film morphology) [10], exploiting metastable phases [11], solid solutions [12], mixed oxides [13] and by optimizing the operation temperature [13]. In fact, high acetone selectivity was found with Si-doped ε-$WO_3$ when operated at 350 °C [11]. This enabled the monitoring of fat burn during exercise and rest in 20 volunteers by measuring acetone in their breath (> 872 compounds) [14]. When combined to an array with ammonia-selective Si-doped α-$MoO_3$ [13] and isoprene-selective Ti:ZnO [12], even sub-ppm concentrations of human breath- and skin-emitted acetone, ammonia and isoprene can be quantified [15].

Here, the effect of *orthogonality* on array performance is investigated experimentally by systematically replacing non-selective $SnO_2$-based sensors in an array by distinctly-selective Si:$MoO_3$ [13] and Si:$WO_3$ [11] for ammonia and acetone, respectively. The arrays are tested with 60 random combinations of ammonia, acetone and ethanol in the ppb to low ppm range at dry conditions. Next, array size and composition is varied systematically to understand the contribution of each sensor on analyte prediction. Finally, the stability of the extracted regression coefficients is evaluated.

# 2. Experimental

### Sensor fabrication and characterization

Different sensing nanoparticles, were produced by flame spray pyrolysis (FSP) and directly deposited [16] onto 15 × 13 × 0.8 mm $Al_2O_3$ substrates featuring interdigitated electrodes (Electronic Design Center, Case Western Reserve University) (figure 1a). For this, the substrate was mounted on a water-cooled holder 20 cm above the burner [17]. The precursor

solutions for Pd:$SnO_2$ (1 mol%) [6], Si:$SnO_2$ (6 mol%) [17], Pt:$SnO_2$ (0.15 mol%) [18], Si:$WO_3$ (10 mol%) [11] and Si:$MoO_3$ (6.9 mol%) [13] were prepared according to the cited literature. The precursors were supplied at a feed rate of 5 mL $min^{-1}$ through a nozzle and dispersed to a fine spray by 5 L $min^{-1}$ oxygen at a pressure drop of 1.5 bar (1.6 bar for Si:$MoO_3$). The spray was ignited by premixed methane / oxygen (1.25 L $min^{-1}$ / 3.2 L $min^{-1}$) flame surrounding the nozzle. Sheath oxygen (5 L $min^{-1}$) was added through an annulus surrounding the flame.

The mechanical stability of the nanoparticle deposits was enhanced by subsequent in situ annealing with a particle-free flame for 30 s [17]. So, the substrate holder was lowered to 14.5 cm above the burner and xylene was fed at 1 L $min^{-1}$ and dispersed with 5 L $min^{-1}$ oxygen. Finally, the sensors were thermally stabilized by annealing in an oven (Carbolite Gero 30-3000 °C) for 10 h at 500 °C (5 h at 450 °C for Si:$MoO_3$) to prevent sintering and thus signal drift during operation. As a result, similar flame-made Pt:$SnO_2$ had shown good long term stability over 20 days at 10% RH [18]. A Hitachi FE-SEM 4000 was used for scanning electron microscopy (SEM) operated at 3 kV.

**Sensor and array testing**

The different sensing materials were assembled to a *conventional* (Pd:$SnO_2$, Si:$SnO_2$, and Pt:$SnO_2$) and an *orthogonal* (Si:$WO_3$, Si:$SnO_2$ and Si:$MoO_3$) array by mounting the sensors on Macor holders [11] and placing them in a Teflon-made chamber (figure S1). Doped $SnO_2$ (400 °C) [6], Si:$WO_3$ (350 °C) [11] and Si:$MoO_3$ (400 °C) [13] were operated at their optimal temperature with respect to analyte sensitivity and selectivity. For this, the sensors were heated up through a Pt heater on the backside of the substrates by supplying constant DC voltages of 15.9 V and 18.2 V for 350 °C and 400 °C, respectively. The temperature was controlled by a Pt temperature resistance detector (RTD) on the front (figure S1c).

Gas tests were performed in an evaluation setup described in detail elsewhere [13]. In brief, dry synthetic air (Pan Gas, $C_nH_m$ and $NO_x \leq 100$ ppb) was used as a carrier and acetone (50 ppm in $N_2$, Pan Gas), ammonia (50 ppm in $N_2$, Pan Gas), and ethanol (50 ppm in $N_2$, Pan Gas) were admixed by calibrated mass flow controllers (Bronkhorst, Netherlands) to obtain the desired gas mixtures at a total flow rate of 1 L $min^{-1}$. In total, 60 different gas mixtures were measured consisting of randomly combined concentrations of ammonia (250, 500, 800, 1200, 1600 and 2000 ppb) [19], acetone (250, 400, 600, 800, 1200 and 1800 ppb) [20] and ethanol (50, 100, 150, 200, 400 and 600 ppb) [20] corresponding to typical human breath concentrations. The applied Si:$WO_3$ sensor had lower limit of detection (at signal-to-noise-ratio of 3) of 2.9 ppb acetone [11], Si:$MoO_3$ of 50.7 ppb ammonia [13] and Si:$SnO_2$ of 0.2 ppb ethanol [6], all at 90% relative humidity (RH). Note that the RH was not included to demonstrate the effect of orthogonality more clearly. However, humidity effects had been assessed already with the single sensors (i.e., Si:$MoO_3$ [13], Ti:ZnO [12], and Si:$WO_3$ [11]) and arrays in simulated gas mixtures (at 90% RH) [6] and for breath- and skin-emissions [15].

**Data analysis**

The film resistance between the interdigitated electrodes was measured continuously by a Multimeter (2700, Keithley). The responses of individual sensors were calculated as follows:

$$S = \frac{R_{air}}{R_{analyte}} - 1 \quad (1)$$

where $R_{air}$ and $R_{analyte}$ denote the resistance measured in dry synthetic air without and with the analytes, respectively. The sensor sensitivity ($\sum$) was defined as the derivative of the sensor response S with respect to the analyte concentration c (IUPAC):

$$\sum = \frac{\partial S}{\partial c} \quad (2)$$

Due to the quite linear calibration curves of the sensors, ∑ is approximated by linear regression over the tested analyte range. The analyte concentrations were predicted with the array by multivariate linear regression (MVLR) [21]. This is a suitable approach due to the linear calibration curves of such sensors [8] at the present concentration range, applied successfully already with similar arrays [6,15]. Furthermore, it allows a clear comparison between different array compositions due to the model's simplicity. Therein, the concentration of an analyte $C_x$ is described as a superposition of each sensor response $S_i$ multiplied with an individual regression coefficient $a_{i,x}$ and intercept $b_x$ where i and n denote the number of sensors in the array.

$$C_x = \sum_{i=1}^{n=5} a_{i,x} S_i + b_x \tag{3}$$

During a 6-fold cross-validation [22], data points were separated into calibration and test sets to assess the performance of the sensor arrays and prevent overfitting. During calibration, the coefficients $a_{i,x}$ and $b_x$ were obtained and then used to predict the concentrations $C_x$ of the test set. Note that array compositions up to n = 5 sensors were tested. According to IUPAC, array accuracy was defined as the difference between the average predicted concentration and the actual one. Array precision was the standard deviation of the predicted concentrations. All calculations were performed with MATLAB (version R2017b, MathWorks, Natick, MA)

# 3. Results and discussion

**Designing selective sensing materials by flame aerosol synthesis**

Figure 1a shows schematically the fabrication and direct deposition of nanoparticles onto $Al_2O_3$ sensor substrates with interdigitated electrodes by FSP. Therein, nanoparticles with distinct composition, crystal phase and size at high purity (similar to optical fibers [23]) are formed in the gas phase and deposited as highly porous nanostructured sensing films. Top-

view SEM of the Si:$SnO_2$ (6 mol%) film (figure 1b) indicates fine networks of aggregated and agglomerated primary particles, typical for such flame-made and directly deposited layers [16]. During FSP, $SnO_2$ forms the cassiterite phase featuring a tetragonal crystal structure (figure 1b, inset) with six coordinated Sn (red) and three coordinated O (grey) [17].

The Si-doping thermally stabilizes $SnO_2$ to prevent grain and particle growth during typical high temperature operation (e.g. 400 °C) [6]. That way, the highly porous and fine film morphology with its large surface area is maintained [17]. This is ideal for gas sensing, as analytes can easily penetrate into the open film structure resulting in fast response (< 1 min) and recovery times (< 4 min) with reproducible sensitivity and reversible responses. In fact, high sensor responses to ammonia are observed already at sub-ppm concentrations (e.g. S = 0.47 at 800 ppb, red squares in figure 1d) with rather linear response characteristics (dotted line), as expected from diffusion-reaction theory [24]. The corresponding sensitivity for the entire ammonia concentration range is 0.57 $ppm^{-1}$. Increasing the acetone concentration in the gas mixture, however, shifts the response curves upwards, while sensitivity is not affected (similar slope for all curves). This indicates substantial cross-sensitivity to acetone, in line with literature [6]. This, however, is an issue for selective ammonia sensing in complex mixtures.

Higher selectivity is found with specifically tailored material compositions, crystal phases and/or morphologies, if not achieved through external filters (e.g., sorption [25] or molecular sieves [26]), preconcentrators [27] or gas chromatography columns [28]). For example, Si-doped $MoO_3$ shows high ammonia selectivity [13]. In this case, the sensing structure consists of larger aggregated nanoparticles (< 100 nm) and needle-like ones up to several µm long (figure 1c). By systematically optimizing the Si doping content the growth of α-$MoO_3$ is prevented at typical operational temperatures (e.g. 400 °C [13]).

That phase is composed of layers of distorted $MoO_6$ octahedra (blue shaded in inset of figure 1c). The corresponding Si:$MoO_3$ sensor exhibits lower responses (figure 1e) and

sensitivity ($\sum$ = 0.31 $ppm^{-1}$) for ammonia but higher selectivity. In specific, the presence of 800 ppb acetone on Si:$MoO_3$ leads to a prediction error of 22% (974 instead of 800 ppb ammonia). This is significantly less compared to Si:$SnO_2$ (119% at the same conditions, figure 1d). Note that 800 ppb of interfering acetone is a realistic scenario in breath analysis at normal conditions [20], while higher concentrations of several ppm can occur during exercise or fasting [29]. Since higher accuracy is needed, further optimization in arrays with statistical response analysis to compensate for such cross-sensitivities is required.

**Sensor selectivity and array orthogonality**

Figure 2a shows normalized responses of Pd:$SnO_2$, Pt:$SnO_2$, Si:$SnO_2$, Si:$WO_3$ and Si:$MoO_3$ to average breath concentrations [30] of ammonia (833 ppb), acetone (477 ppb) and ethanol (112 ppb). The $SnO_2$-based sensors are widely sensitive and respond to all analytes, in agreement with literature [31,6]. Even when doping $SnO_2$ with different elements (i.e. Pt group metals vs. Si), only small selectivity alterations are obtained that result in quite similar response patterns. The collinearity of these sensors is better visualized by displaying each sensor's responses as unit vector in a 3-D analyte space with acetone, ammonia and ethanol representing the axes (figure 2b). For the $SnO_2$-based sensors the response vectors nearly align, in particular, the Pd:$SnO_2$ (orange) and Si:$SnO_2$ (light blue) almost overlap. In fact, they differ only by an angle of 2° while the Pt:$SnO_2$ (green) and Pd:$SnO_2$ or Pt:$SnO_2$ and Si:$SnO_2$ are separated by about 10°. When utilizing such rather similar or collinear sensors in an array configuration (denoted here as *conventional* array), the close alignment results in a high degree of collinearity even though being linearly independent. This can lead to unstable regression coefficients during MVLR: small measurement errors in sensor response result in large deviations in the estimated concentrations [8]. Overall, such sensor arrays feature low discrimination power resulting in weak analyte estimations and strong sensitivity to small

changes in background gases, humidity or temperature [9]. This makes the device only reliable within the calibrated gas mixture, if at all [32,9].

To increase the degree of orthogonality, enhanced selectivity variance within the array is needed. This can be accomplished by exchanging collinear sensors (Pt:$SnO_2$ and Pd:$SnO_2$) with distinctly selective ones (Si:$WO_3$ and Si:$MoO_3$). For these materials, the strong selectivity variance is obtained by changing the base metal oxide (from $SnO_2$ to $WO_3$ and $MoO_3$). For Si:$WO_3$, this results in higher acetone selectivity over ammonia and ethanol (figure 2a). At the same time, Si:$MoO_3$ exhibits higher ammonia selectivity (figure 2a). Together with non-specific Si:$SnO_2$ they combine to an array (denoted here as *orthogonal*), where all vectors are clearly separated by angles ranging from 23 to 64° (figure 2c).

This leads to a significantly higher degree of orthogonality, also visualized by the spanned area of the vectors (grey shaded) [9]. Hence, this *orthogonal* configuration should feature regression coefficients with increased stability, higher discrimination power between the analytes and therefore lead to more accurate and precise estimations for all analytes [8].

**Array performance in gas mixtures**

Both array configurations are "trained" and tested (6-fold cross-validation) with 60 random combinations of acetone (250 – 1800 ppb) [20] ammonia (250 – 2000 ppb) [19], and ethanol (50-600 ppb) [20] occurring typically in the breath of healthy humans. Figure 3 shows the array-estimated ammonia (a), ethanol (b), and acetone (c) concentrations over the actual ones in these mixtures. Note that symbols and error bars indicate the average concentrations and standard deviations, respectively, of the *conventional* (red circles) and the *orthogonal* array (green squares). The *conventional* array estimates ammonia and ethanol with large error bars and even fails to resolve increasing concentrations, as evident from the low coefficients of determination ($R^2$) of 0.01 and 0.28, respectively. In particular for ammonia, the average levels are consistently estimated around 1000 ppb (figure 3a), despite the actual variations

between 250-2000 ppb. The poor array performance is also reflected in the low accuracy (large deviation from the dotted line) and low precision (large error bar), for instance at 800 ppb of ammonia with values of 272 and 240 ppb, respectively, corresponding to an average error of 34%. Only for acetone, different concentrations are recognized better ($R^2$ = 0.88, figure 3c) but errors increase at high concentrations (i.e. 1800 ppb). Note that increasing the number of calibration points of the conventional array does not improve the array performance (see figure S2).

Most importantly, the *orthogonal* array estimates all analytes significantly better with outstanding $R^2$ of 0.96, 0.88 and 0.99 for ammonia, ethanol and acetone, respectively. This strong array performance is a remarkable improvement compared to that of the *conventional* array. For instance at 800 ppb ammonia, the accuracy and precision are 53 and 85 ppb, respectively. This corresponds to an average error of 6.6%, which is much smaller than the 34% of the conventional array. That can have significant impact on breath analysis where ammonia is an important marker to detect end-stage renal disease in humans and such low concentration differences need to be resolved especially to detect early stages [19].

**Influence of array size and composition on estimation performance**

To understand the improved performance of the *orthogonal* array, the role of each sensor on adjusted $R^2$ is investigated exemplarily for ammonia in figure 4. Note that the adjusted $R^2$ is calculated to account for the different number of sensors [33]. Data for all additional sensor combinations and other analytes are shown in figure S3. The Si:$SnO_2$ sensor alone fails to resolve different ammonia concentrations, as indicated by the low adjusted $R^2$ of 0.01 and expected from the strong interference of the other analytes (figures 1d & 2a). When adding Pd:$SnO_2$ and Pt:$SnO_2$ this is not improved and the adjusted $R^2$ even decreases, most likely due to high collinearity (figure 2b) and the resulting amplification of noise [9]. This is in line with the poor ammonia estimation of the *conventional* array (figure 3a).

In contrast, Si:$MoO_3$ allows a much better ammonia estimation (adjusted $R^2$ of 0.68) already as *single sensor* than the $SnO_2$-based sensors and arrays due to its higher ammonia selectivity (figures 1e & 2a). This is even improved when adding Si:$SnO_2$ to it (adjusted $R^2$ of 0.76), due to their different selectivities (compare red and light blue vectors in figure 2c). This results in a higher discrimination power and therefore a better analyte estimation [9]. The prediction can be enhanced further by adding the Si:$WO_3$ sensor, resulting in an adjusted $R^2$ of 0.96 (figure 4). As a result, the high discrimination power of an array consisting of sensors with distinct selectivities allows analyte estimations unachievable by conventional arrays. Out of curiosity also the combination of all 5 sensors was tested but the adjusted $R^2$ (0.97) hardly increases further compared to the *orthogonal* design, showing again the redundant role of collinear sensors.

**Regression coefficients: significance and robustness**

Another indicator of the role of a sensor within an array is the stability of its regression coefficient in the statistical model (i.e. $a_{i,x}$ in eq. 2 for MVLR, see Experimental) [34]. Figure 5 shows the regression coefficients for all sensors in the *conventional* (a-c) and *orthogonal* (d-e) arrays for the prediction of ammonia (a, d), acetone (b, e) and ethanol (c, f) concentrations. Error bars represent the variability during calibration, i.e. the change in regression coefficient when successively adding more data points in the least squares algorithm. The error bar in relation to the absolute value of a regression coefficient is indicative for the robustness against interfering concentrations thus stability and overall significance of a sensor in the array [35]. From these, also *p*-values can be computed as indicator of significance, most often used for further array optimization (e.g. by removing the least significant sensor, so called backward-elimination) [34].

For the *conventional* design (figure 5a-c), the regression coefficients exhibit rather large error bars for all analytes. These are especially pronounced for ammonia (figure 5a) correlating

with the poor analyte estimation of the *conventional* array (figure 3). Furthermore, the error bars of the Pd:$SnO_2$ cross the zero-line (dashed) consistently for all analytes (figure 5a-c) revealing the insignificant role of this sensor. This is further supported by the high *p*-values (all above 0.6), an indication that this sensor introduces rather noise than new information [9]. As a result, this sensor is redundant for all analyte estimations, most likely due to its high collinearity with the Si:$SnO_2$ sensor (compare orange and light blue vectors in figure 2b).

The error bars of the *orthogonal* array (d-f) are significantly smaller for all analytes than for the *conventional* one (a-c). This is in line with theory [34], where a higher degree of orthogonality (grey shaded triangles in figures 2b,c) should result in more stable regression coefficients leading to increased discrimination power, accuracy and precision of the device, as demonstrated already in figure 3. Note that the acetone coefficients of the *conventional* array (figure 5b), exhibiting the smallest error bars of the 3 analytes, already allow for an accurate quantification of acetone (figure 3c). Nevertheless, increased stability is still achieved in the *orthogonal* design (figure 5e) resulting in an improved performance (figure 3c).

# 4. Conclusions

We provide experimental evidence that sensor array performance depends largely on the orthogonality of its constituent sensors. Utilizing distinctly selective sensors in arrays improved discrimination power and stability of the regression coefficients, necessary for accurate and precise analyte predictions in relevant gas mixtures. In specific, in mixtures of ammonia, acetone and ethanol, $R^2$ of 0.96, 0.99 and 0.88 are achieved, respectively. Such highly selective sensing materials are accessible with state-of-the-art fabrication methods by exploiting, for instance, unique material composition, morphologies or metastable crystal phases.

In contrast, integrating collinear sensors into arrays (conventional array) hardly improved or even decreased performance, probably due to amplification of noise. This resulted in low discrimination power and inability to distinguish different analyte concentrations in mixtures ($R^2$ of 0.01 for ammonia, 0.86 for acetone and 0.28 for ethanol). As a result, this study highlights the importance of selective sensing material engineering and their integration into arrays to overcome accuracy and precision restrictions.

## Acknowledgments

This study was financially supported by the Swiss National Science Foundation (Grant No.170729 & 159763) and by an ETH Research Grant (No. ETH-21 18-1).

## References

1. Persaud K, Dodd G (1982) Analysis of discrimination mechanisms in the mammalian olfactory system using a model nose. Nature 299 (5881):352-355. doi:10.1038/299352a0
2. Röck F, Barsan N, Weimar U (2008) Electronic nose: current status and future trends. Chem Rev 108 (2):705-725. doi:10.1021/cr068121q
3. Ragazzo-Sanchez JA, Chalier P, Chevalier D, Ghommidh C (2006) Electronic nose discrimination of aroma compounds in alcoholised solutions. Sensor Actuat B-Chem 114 (2):665-673. doi:10.1016/j.snb.2005.05.032
4. Phillips M (2005) Can the electronic nose really sniff out lung cancer? Am J Respir Crit Care Med 172 (8):1060; author reply 1060-1061. doi:10.1164/ajrccm.172.8.959
5. Pizzini A, Filipiak W, Wille J, Ager C, Wiesenhofer H, Kubinec R, Blaško J, Tschurtschenthaler C, Mayhew CA, Weiss G, Bellmann-Weiler R (2018) Analysis of volatile organic compounds in the breath of patients with stable or acute exacerbation of chronic obstructive pulmonary disease. J Breath Res 12 (3):036002. doi:10.1088/1752-7163/aaa4c5
6. Güntner AT, Koren V, Chikkadi K, Righettoni M, Pratsinis SE (2016) E-nose sensing of low-ppb formaldehyde in gas mixtures at high relative humidity for breath screening of lung cancer? ACS Sens 1 (5):528-535. doi:10.1021/acssensors.6b00008
7. Sundgren H, Winquist F, Lukkari I, Lundstrom I (1991) Artificial neural networks and gas sensor arrays - quantification of individual components in a gas-mixture. Meas Sci Technol 2 (5):464-469. doi:10.1088/0957-0233/2/5/008
8. Carey WP, Beebe KR, Sanchez E, Geladi P, Kowalski BR (1986) Chemometric analysis of multisensor arrays. Sensors and Actuators 9 (3):223-234. doi:10.1016/0250-6874(86)80023-3
9. Pearce TC, Schiffman SS, Nagle HT, Gardner JW (2003) Handbook of machine olfaction: electronic nose technology. WiILEY-VCH, Weinheim. doi:10.1002/3527601597

10. Joshi N, Hayasaka T, Liu YM, Liu HL, Oliveira ON, Lin LW (2018) A review on chemiresistive room temperature gas sensors based on metal oxide nanostructures, graphene and 2D transition metal dichalcogenides. Microchim Acta 185 (4). doi:10.1007/s00604-018-2750-5
11. Righettoni M, Tricoli A, Gass S, Schmid A, Amann A, Pratsinis SE (2012) Breath acetone monitoring by portable Si:$WO_3$ gas sensors. Anal Chim Acta 738:69-75. doi:10.1016/j.aca.2012.06.002
12. Güntner AT, Pineau NJ, Chie D, Krumeich F, Pratsinis SE (2016) Selective sensing of isoprene by Ti-doped ZnO for breath diagnostics. J Mater Chem B 4 (32):5358-5366. doi:10.1039/C6TB01335J
13. Güntner AT, Righettoni M, Pratsinis SE (2016) Selective sensing of $NH_3$ by Si-doped α-$MoO_3$ for breath analysis. Sensor Actuat B-Chem 223:266-273. doi:10.1016/j.snb.2015.09.094
14. Güntner AT, Sievi NA, Theodore SJ, Gulich T, Kohler M, Pratsinis SE (2017) Noninvasive body fat burn monitoring from exhaled acetone with Si-doped $WO_3$-sensing nanoparticles. Anal Chem 89 (19):10578-10584. doi:10.1021/acs.analchem.7b02843
15. Güntner AT, Pineau NJ, Mochalski P, Wiesenhofer H, Agapiou A, Mayhew CA, Pratsinis SE (2018) Sniffing entrapped humans with sensor arrays. Anal Chem 90 (8):4940-4945. doi:10.1021/acs.analchem.8b00237
16. Mädler L, Roessler A, Pratsinis SE, Sahm T, Gurlo A, Barsan N, Weimar U (2006) Direct formation of highly porous gas-sensing films by in situ thermophoretic deposition of flame-made Pt/$SnO_2$ nanoparticles. Sensor Actuat B-Chem 114 (1):283-295. doi:10.1016/j.snb.2005.05.014
17. Tricoli A, Graf M, Pratsinis SE (2008) Optimal doping for enhanced $SnO_2$ sensitivity and thermal stability. Adv Funct Mater 18 (13):1969-1976. doi:10.1002/adfm.200700784
18. Mädler L, Sahm T, Gurlo A, Grunwaldt JD, Barsan N, Weimar U, Pratsinis SE (2006) Sensing low concentrations of CO using flame-spray-made Pt/$SnO_2$ nanoparticles. J Nanopart Res 8 (6):783-796. doi:10.1007/s11051-005-9029-6
19. Davies S, Spanel P, Smith D (1997) Quantitative analysis of ammonia on the breath of patients in end-stage renal failure. Kidney Int 52 (1):223-228. doi:10.1038/ki.1997.324
20. Diskin AM, Spanel P, Smith D (2003) Time variation of ammonia, acetone, isoprene and ethanol in breath: a quantitative SIFT-MS study over 30 days. Physiol Meas 24 (1):107-119. doi:10.1088/0967-3334/24/1/308
21. Mardia KV, Kent JT, Bibby JM (1979) Multivariate analysis. Academic Press, Cambridge
22. James G, Witten D, Hastie T, Tishirani R (2013) An introduction to statistical learning. Springer, Heidelberg. doi:0.1007/978-1-4614-7138-7
23. Pratsinis SE (2010) Aerosol-based technologies in nanoscale manufacturing: from functional materials to devices through core chemical engineering. AIChE J 56 (12):3028-3035. doi:10.1002/aic.12478
24. Gardner JW (1989) A diffusion-reaction model of electrical-conduction in tin oxide gas sensors. Semicond Sci Tech 4 (5):345-350. doi:10.1088/0268-1242/4/5/003
25. van den Broek J, Güntner AT, Pratsinis SE (2018) Highly selective and rapid breath isoprene sensing enabled by activated alumina filter. ACS Sens 3 (3):677-683. doi:10.1021/acssensors.7b00976
26. Güntner AT, Abegg S, Wegner K, Pratsinis SE (2018) Zeolite membranes for highly selective formaldehyde sensors. Sensor Actuat B-Chem 257:916-923. doi:10.1016/j.snb.2017.11.035
27. McCartney MM, Zrodnikov Y, Fung AG, LeVasseur MK, Pedersen JM, Zamuruyev KO, Aksenov AA, Kenyon NJ, Davis CE (2017) An easy to manufacture micro gas preconcentrator for chemical sensing applications. ACS Sens 2 (8):1167-1174. doi:10.1021/acssensors.7b00289

28. Itoh T, Miwa T, Tsuruta A, Akamatsu T, Izu N, Shin W, Park J, Hida T, Eda T, Setoguchi Y (2016) Development of an exhaled breath monitoring system with semiconductive gas sensors, a gas condenser unit, and gas chromatograph columns. Sensors 16 (11). doi:10.3390/s16111891
29. Anderson JC (2015) Measuring breath acetone for monitoring fat loss: review. Obesity 23 (12):2327-2334. doi:10.1002/oby.21242
30. Smith D, Turner C, Spanel P (2007) Volatile metabolites in the exhaled breath of healthy volunteers: their levels and distributions. J Breath Res 1 (1):014004. doi:10.1088/1752-7155/1/1/014004
31. McAleer JF, Moseley PT, Norris JOW, Williams DE, Taylor P, Tofield BC (1987) Tin oxide based gas sensors. Mater Chem Phys 17 (6):577-583. doi:10.1016/0254-0584(87)90017-4
32. Gardner JW, Boilot P, Hines EL (2005) Enhancing electronic nose performance by sensor selection using a new integer-based genetic algorithm approach. Sensor Actuat B-Chem 106 (1):114-121. doi:10.1016/j.snb.2004.05.043
33. Olive DJ (2017) Linear regression. Springer, Heidelberg. doi:10.1007/978-3-319-55252-1
34. Harrell FE (2001) Regression Modeling Strategies. Springer Series in Statistics. Springer, Heidelberg. doi:10.1007/978-1-4757-3462-1
35. King G (1986) How not to lie with statistics - avoiding common mistakes in quantitative political-science. Am J Polit Sci 30 (3):666-687. doi:10.2307/2111095

## Figures and Captions

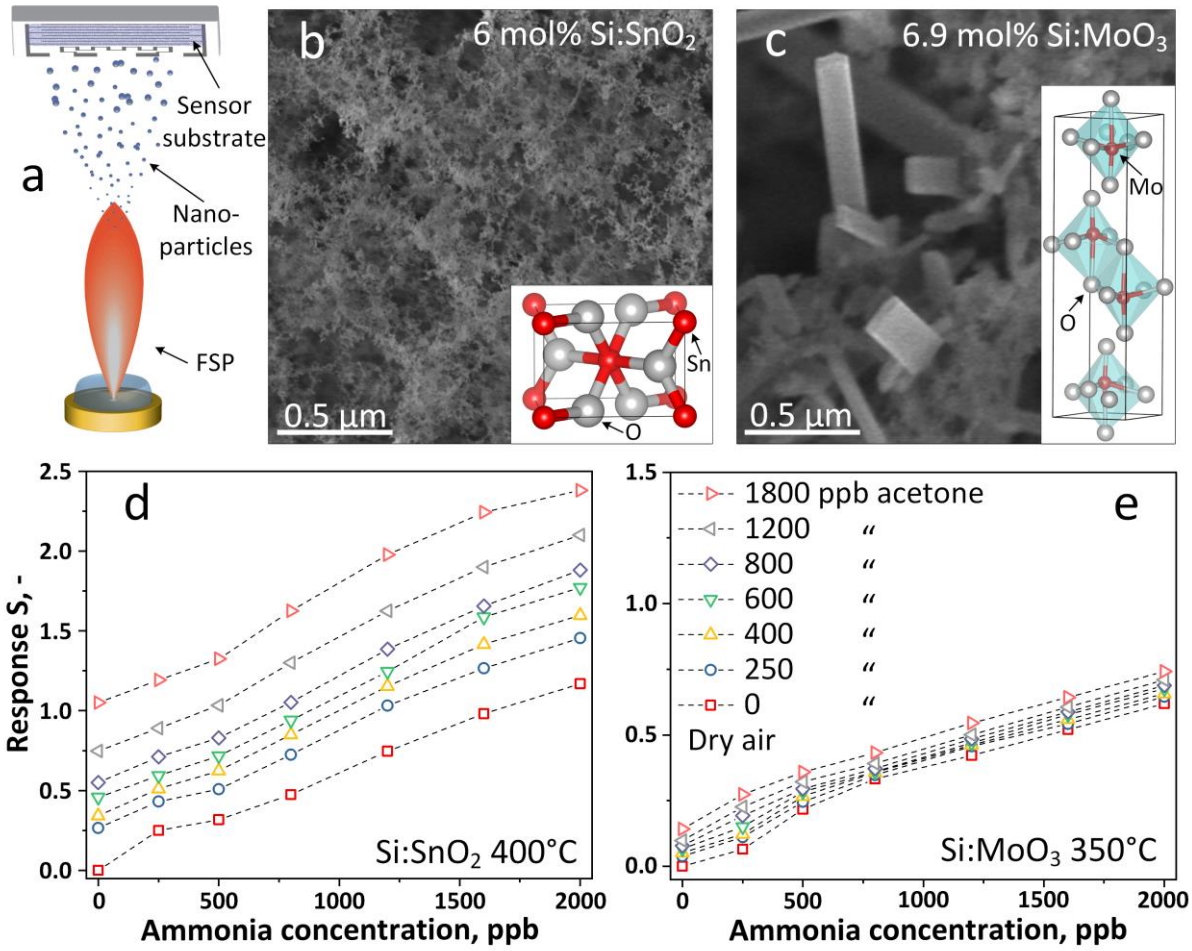


**Figure 1 |** (a) Sensing nanoparticles are produced by flame spray pyrolysis (FSP) and are deposited directly onto sensor substrates. SEM image (top view) of highly porous (b) Si:$SnO_2$ and (c) Si:$MoO_3$ films. Each sensing material features a distinct composition, morphology and crystal structure (insets) affecting analyte sensitivities, and thus selectivity. Sensor responses of (d) Si:$SnO_2$ and (e) Si:$MoO_3$ to ammonia (0-2000 ppb) at various interfering acetone concentrations (0-1800 ppb).

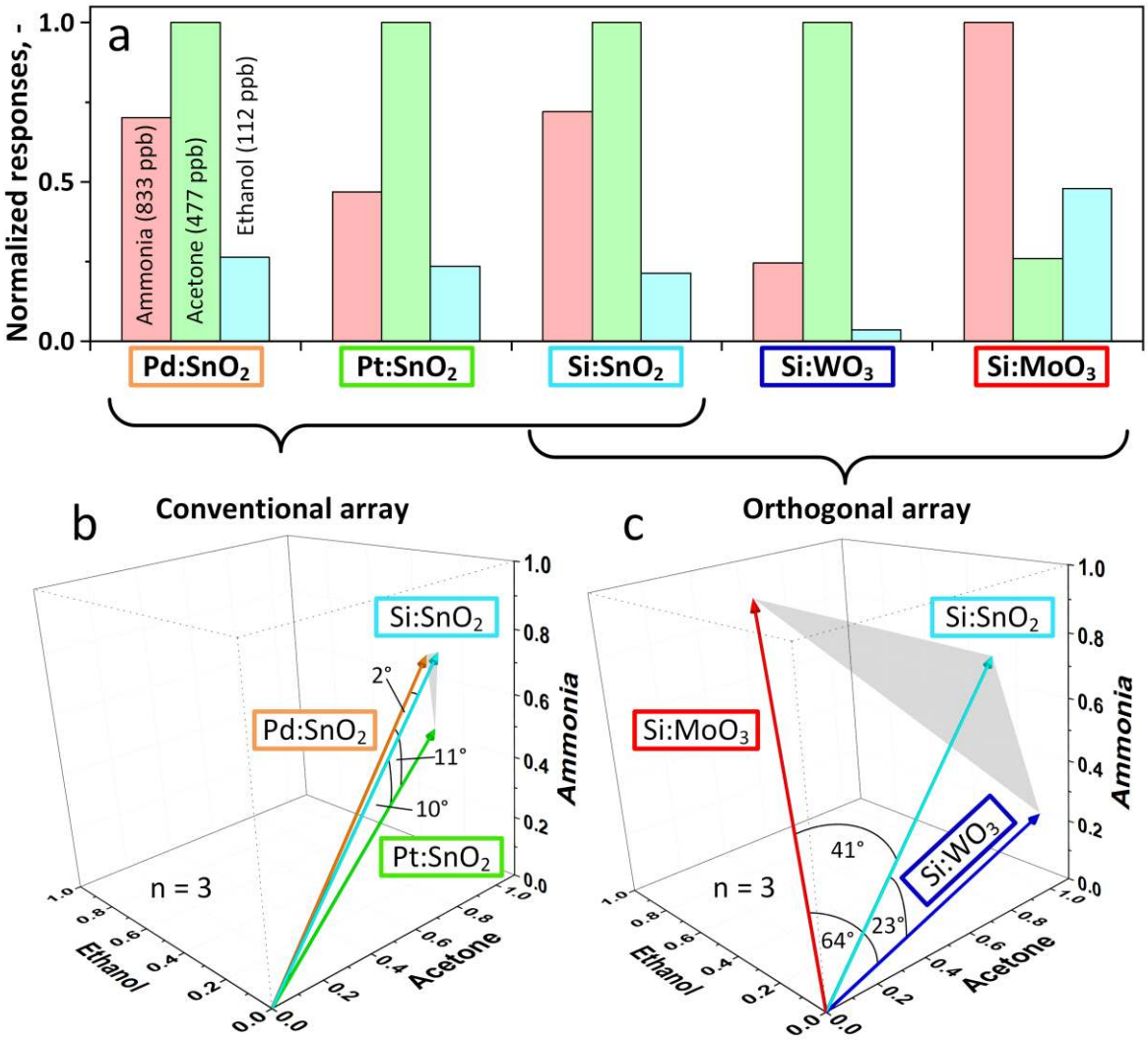


**Figure 2 |** (a) Normalized responses for breath-average (healthy) relevant concentrations of ammonia (833 ppb, red), acetone (477 ppb, green) and ethanol (112 ppb, blue) of $Pd:SnO_2$, $Pt:SnO_2$, $Si:SnO_2$, $Si:WO_3$ and $Si:MoO_3$ sensors. Note that responses are normalized to the maximum of each sensor for a better comparability of the selectivity. The collinearity of the sensors is visualized by showing their normalized responses as unit vectors in a 3-D analyte space for the (b) conventional and (c) orthogonal array designs with sensor compositions as indicated. The degree of orthogonality is indicated by their spanned areas (grey shaded).

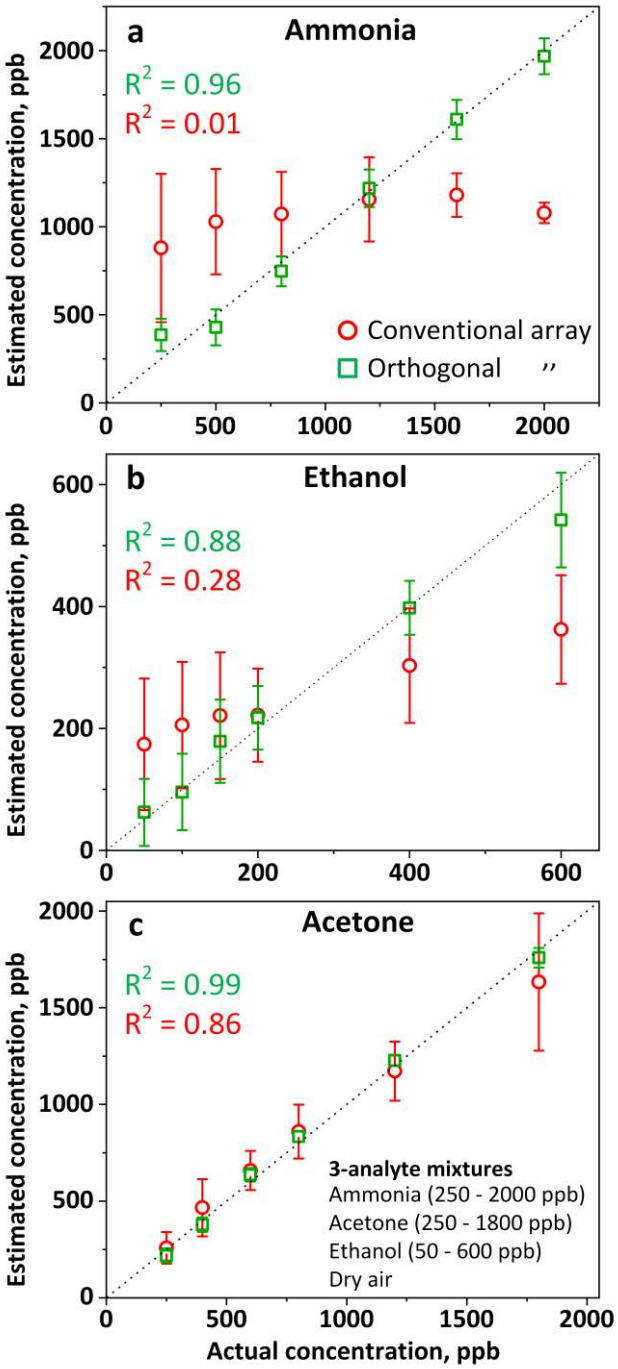


**Figure 3 |** Sensor array estimation of the conventional (red circles) and orthogonal designs (green squares) for (a) ammonia, (b) ethanol and (c) acetone concentrations in 60 different 3-analyte mixtures. Symbols and error bars represent the average and standard deviation of the estimated concentrations, respectively.

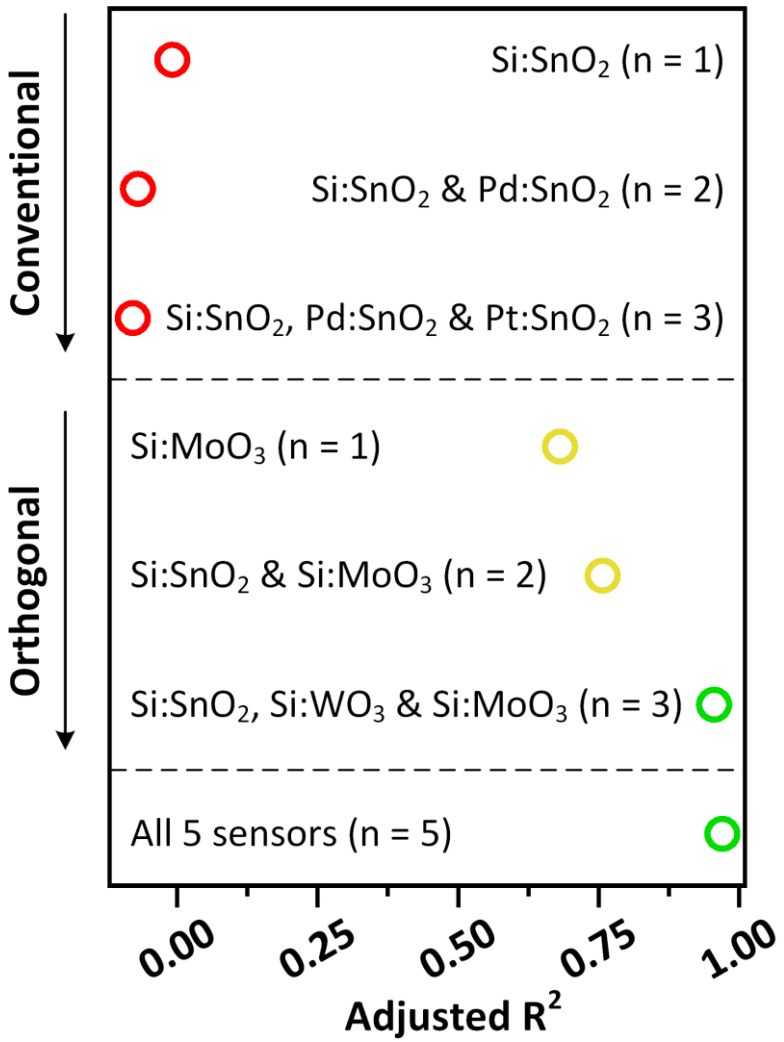


**Figure 4 |** Ammonia estimation performance (adjusted $R^2$) in 3-analyte mixtures by singe sensors and arrays of 2 - 5 sensors. Note that that the adjusted $R^2$ is calculated to account for the different number of sensors. Improved performance is depicted from red (> 0.25) over yellow to green (< 0.85).

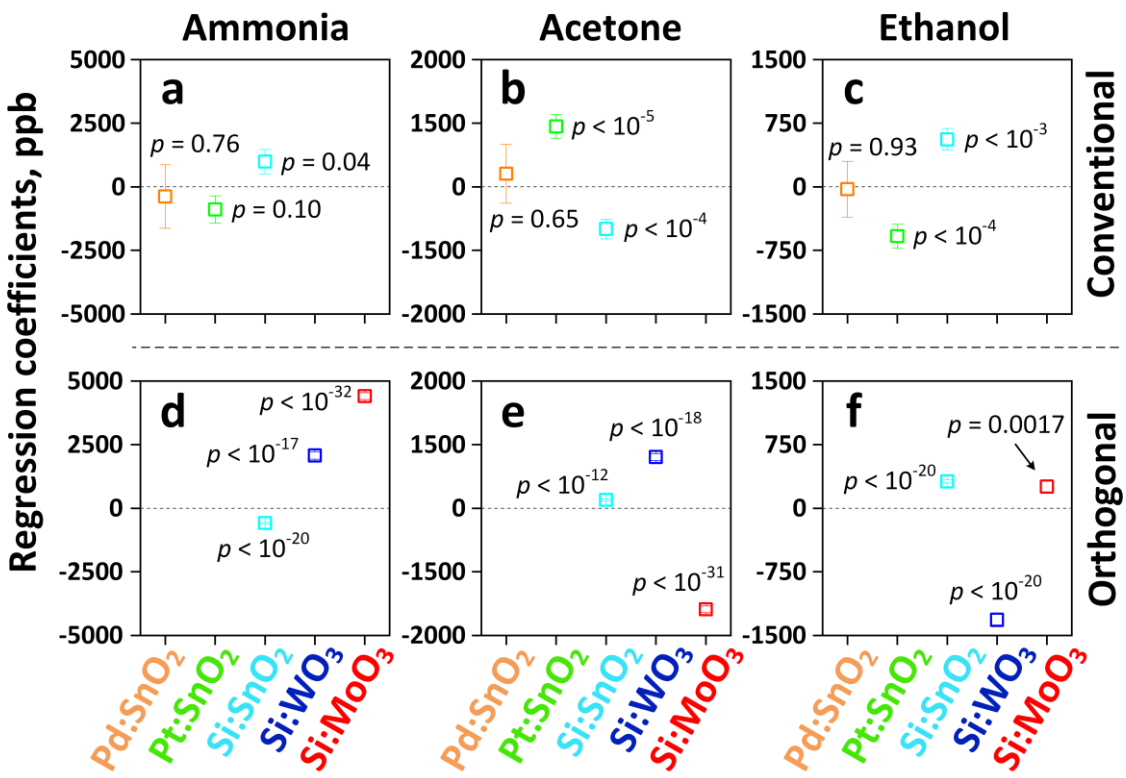


**Figure 5 |** Regression coefficients for the conventional (a-c) and orthogonal (d-f) arrays. The error bars represent the variability during calibration shown along with *p*-values.